PREPRINT

MEASURING THE SPECTRAL COMPONENTS OF SOLAR RADIATION

Frank Bason, SolData
Linåbakken 13, DK-8600 Silkeborg
fax: +45-86 84 15 97

To be presented at the Australia-New Zealand Solar Energy Society
Conference SOLAR '95, Hobart, Tasmania, Nov. 28-Dec. 1, 1995

Abstract

The measurement of the spectral components of solar radiation is a difficult and challenging aspect of solar radiation measurement with important environmental implications [1]. This paper addresses the availability of reliable solar spectral radiation data and techniques for performing measurements [2]. A practical and inexpensive solar radiometer useful in the 300 to 1100 nanometer spectral range is described and the results of preliminary measurements are presented.

The SolData type 95 radiometer employs interference filters and sensitive phototransistors operating in photoconductive mode. This solution offers a low noise, inexpensive alternative to other spectral irradiance measurement options. The design and performance of this device is described in this paper.

The ability to perform continuous measurements of the solar spectral irradiance is useful in connection with perfomance assessments of photovoltaic systems, hazard evaluations of ultraviolet radiation and the measurement of atmospheric trace gases such as ozone.

BACKGROUND

Considerable public attention has been directed at the excess or deficiency of a number of important atmospheric constituents. Water vapor is perhaps the most important example. Excessive carbon dioxide has been identified with the process of global warming due to the absorption of long wave radiation. The reduced concentration of ozone in the stratosphere permits additional ultraviolet (UV) radiation to reach the surface of the earth where it affects plant and animal life. For example, enhanced UV levels can cause growth reduction in conifers and malignant melanoma in humans.

One of the most important means of obtaining information about the distribution and concentration of atmospheric constituents is by observation of direct solar radiation at selected wavelengths. This paper describes an inexpensive device for performing such measurements. Ozone can be studied by measuring solar radiation at 310, 330, 500, 610 and 675 nanometers. Important wavelengths for water vapor measurements are 540 and 940 nm.

Sensitive silicon photodetectors are available to detect photons with wavelengths from about 250 nm to a limiting wavelength of about 1100 nm. They are therefore well suited for measuring the wavelengths noted above. In order to detect radiation at a specific wavelength, narrow-band interference filters (with bandwidths of typically 6 to 8 nanometers) can be used. It is important that all other wavelengths be effectively rejected, so that only radiation close to the wavelength of interest is detected. Off-band wavelengths should be attenuated by a factor of 10^6 or more. With these important components available, an inexpensive but effective solar radiometer can be constructed.

DESIGN CONSIDERATIONS

Detector linearity

According to semiconductor theory, the photocurrent I_{ph} generated by a biased photodetector for a given radiation wavelength should be proportional to the photon flux Φ [3]. If q is the carrier charge, η is the quantum efficiency and G is the photoconductive gain [4], then

$$I_{ph} = \phi \cdot q \cdot \eta \cdot G \quad (1)$$

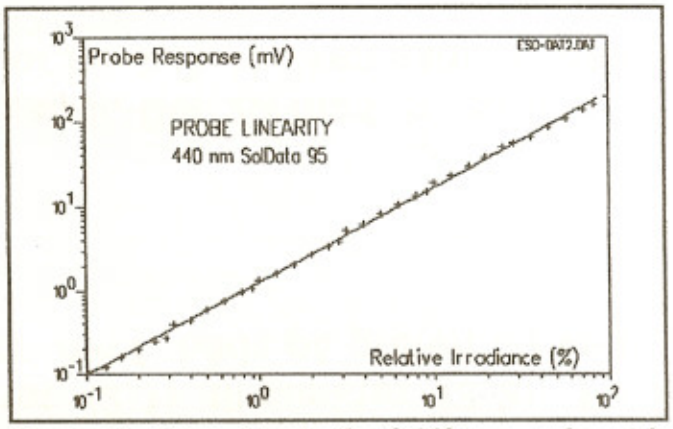

Figure 1: *Linearity check of 440 nm probe with a 150 W halogen light source and a pair of neutral density filter wheels.*

Note that in this expression the product $\eta \cdot G$ corresponds to the probability that a photon incident on the detector will produce a charge carrier which contributes to the photocurrent. Figure 1 shows some experimental measurements with the photodetector used in the solar radiometer. The response, measured in this case for a 440 nm probe, is in fact a linear function of the irradiance of the incident light. A wide range of irradiance levels was obtained by means of a dual neutral density filter wheel [5] and the photocurrent was measured using an IL1700 Research Radiometer [6].

Spectral responsivity

The spectral responsivity characteristics of the photoconductor in use are important to the design of the solar radiometer. In the ideal case, the quantum efficiency of the photoconductor should be independent of wavelength λ up to a critical wavelength λ_C corresponding to the semiconductor bandgap energy E_G:

$$\lambda_C = \frac{h \cdot c}{E_G} = \frac{1240\ nm}{E_G\ (eV)} \quad (2)$$

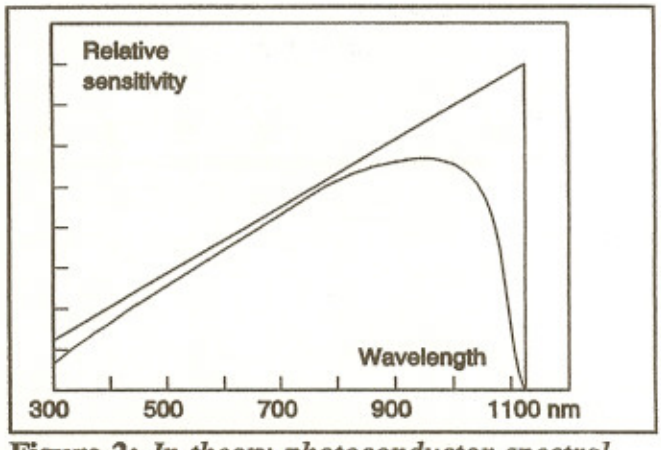

Figure 2: *In theory photoconductor spectral responsivity is proportional to the wavelength λ of the incident radiation up to λ_C.*

where h i Planck's constant and c is the speed of light. The maximum detectable wavelength can be determined when the semiconductor bandgap energy in electron volts (eV) is known. For example in the case of silicon with $E_G \approx 1.11$ eV, the maximum detectable photon wavelength would be about 1120 nm. An elementary calculation of the expected spectral responsivity $S(\lambda)$ predicts that the responsivity should be proportional to the photon wavelength up to λ_C [7]:

$$S = \frac{q \cdot \eta \cdot G}{h \cdot c} \lambda \quad (3)$$

The upper graph in Figure 2 shows the simple linear model. The lower curve shows what

might be expected due to the optical properties of silicon, semiconductor impurities and grain boundaries. Figure 3 shows actual measurements performed on the photodetector used in SolData solar radiometers. The radiometer probes employ interference filters to select specific wavelengths of interest with a bandwidth of about 8 nm. Neutral density filters are used to correct for the varying spectral responsivity of the photodetector, so that probe output signals do not saturate and are compatible with the voltage range of the data collection equipment.

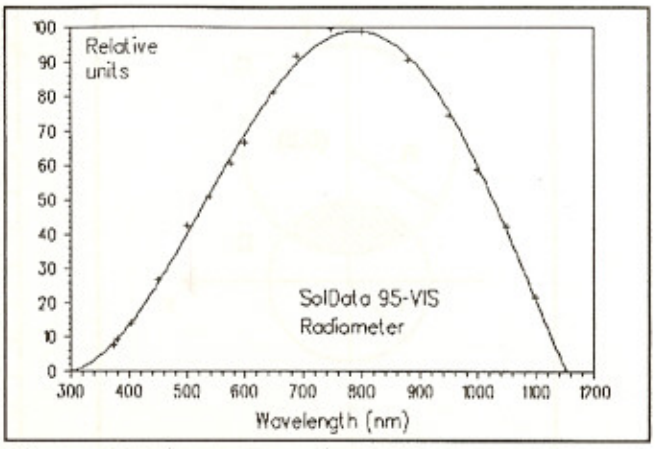

Figure 3: *The measured relative spectral response of the detector from 300-1200 nanometers is shown here.*

Probe geometry and aperture selection

The individual radiometer probes consist of the following optical elements:

- A *collimator* with a circular aperture. The aperture diameter is selected to provide for appropriate angular acceptance characteristics. WMO (the World Meteorological Organization) recommends that a 1:10 ratio of collimator aperture to collimator-detector distance be used for pyrheliometric measurements.
- A *narrow-band inteference filter*. The specific properties of the filters will be described in greater detail shortly.
- A *detector aperture*. This aperture is positioned just in front of the photodetector and is crucial to probe directional responsivity characteristics.
- *Neutral density filters*. It is important that the probe responsivity lies within the linear region when exposed to intense solar radiation. If the photon flux reaching the detector is too great, saturation will occur. Appropriate ND filters must be inserted depending upon the pass-band wavelength and detector sensitivity.

Figure 4 shows these optical elements and their geometry. The rear portion of the probe contains a simple bias circuit and electrical connections to the photodetector and to a cable connector. The probe body is machined from a 30x70 mm aluminum cylinder. Standard tripod mounting hardware is provided for using the probes individually in a calibration setup or for mounting them in an array to create the solar radiometer configuration.

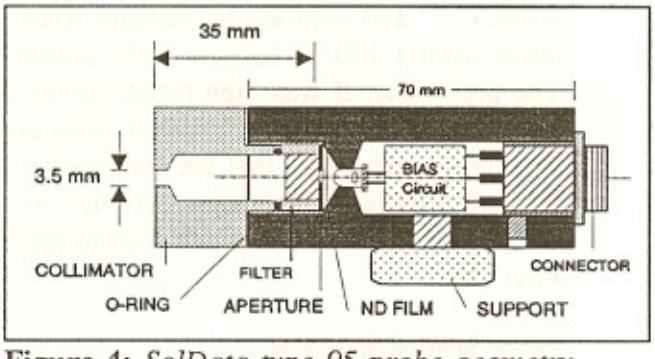

Figure 4: *SolData type 95 probe geometry.*

Figure 5 shows how an illuminated disk of light which has passed through the collimator aperture with diameter D will appear at the detector aperture with diameter d just in front of the detector. The effective overlap area can be computed by an appropriate integration. Notice that the directional responsivity function due to the area overlap factor becomes flatter and flatter as the detector aperture diameter is reduced. There is a complementary relationship between the uniformity of directional response and probe sensitivity. Notice that the limiting case of a "perfectly flat" acceptance angle corresponds to an infinitely

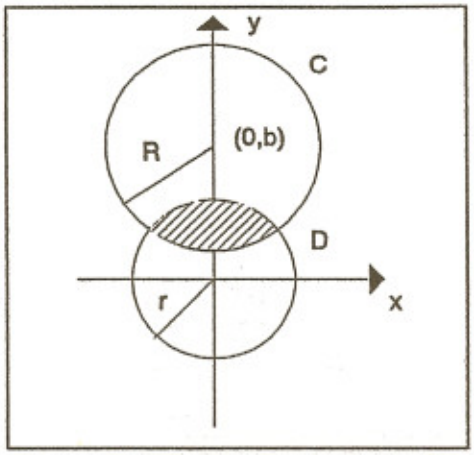

Figure 5: *The lower circle is the probe detector aperture.*

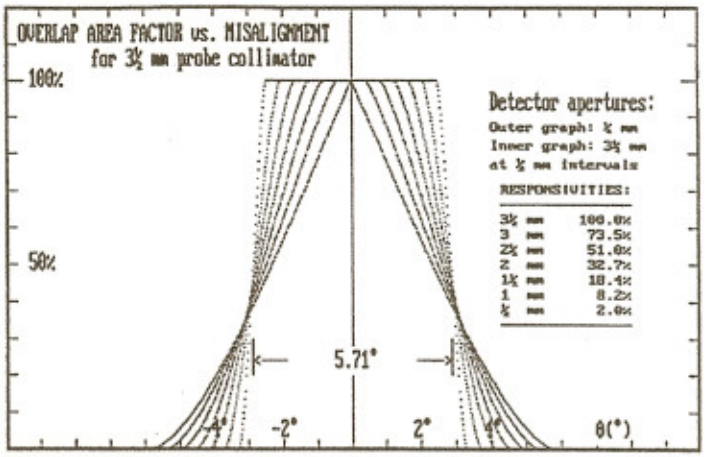

Figure 6: *Geometrical responsivity versus a range of detector aperture diameters.*

small detector aperture. Unfortunately the detector sensitivity approaches zero in this case. With a 3½ mm collimator aperture it turns out that a 2 mm diameter detector aperture is a good compromise in this trade-off.

The overlap area can be calculated as a function of the deviation angle Θ between the probe axis and uniform parallel rays of illumination. In addition to this geometrical effect, the properties of the interference filter will cause the directional responsivity to fall for off-axis probe alignment. Figure 7 shows typical results of actual measurements performed on a probe. The probe was mounted on a goniometer with an angular resolution of about 0.1° and exposed to uniform irradiance from a 150 W halogen light source. The probe output was then measured as a function of the angular deviation from on-axis alignment. Note that the sensitivity falls off slowly at first, primarily due to the physical properties of the transmission filter [8].

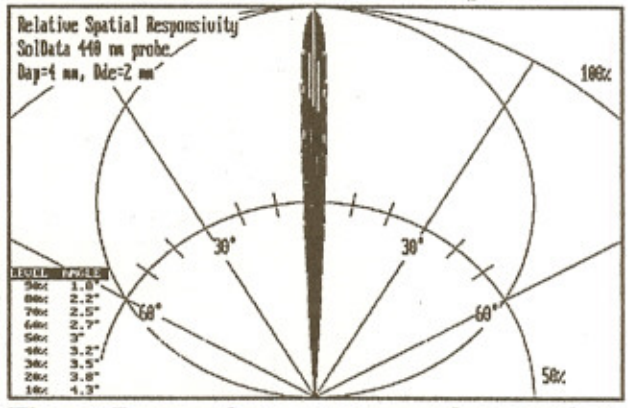

Figure 7: *Actual measurements for a probe with a collimator aperture of 3½ mm and a 2 mm detector aperture.*

Filter transmittivities

Here is a typical double monochromator scan of the transmission characteristics of a radiometer interference filter. The peak wavelength tolerance is typically ±2 nm, and the half maximum band width is 6 to 8 nanometers. The off-band transmittance is less than 10^{-6} from X-ray wavelengths to the far infrared.

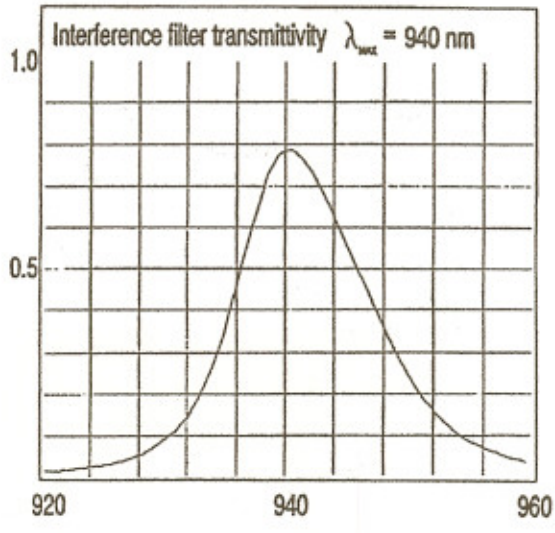

Figure 8: *940 nm filter transmittivity.*

We have used interference filters ranging from 310 nm to 1020 nm, all well within the sensitivity range of the silicon photodetector, with good results. Fortunately, the sun is such an intense light source that it is possible to obtain useful data over nearly the entire range of silicon junction sensitivity.

SOLAR RADIOMETER CONFIGURATION

In order to perform useful measurements the probes described in the previous section must be arranged in an appropriate array, mounted on a solar tracker, provided with appropriate bias voltages and connections, and connected to a data acquisition system.

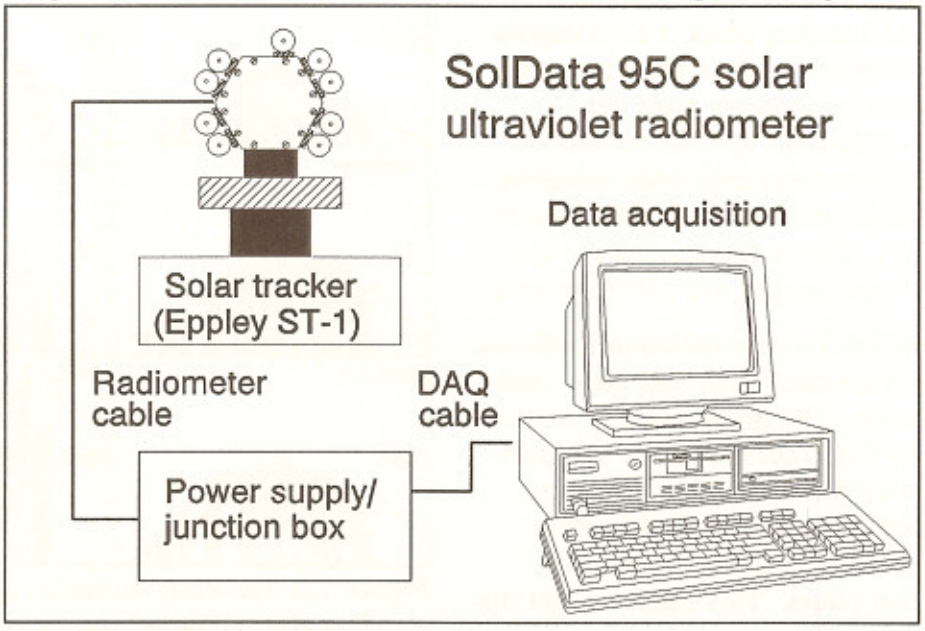

Figure 9: *Typical radiometer configuration with data acquisition.*

Figure 9 shows a typical solar radiometer setup. In the case shown here the probes were mounted on a hexagonal cylinder as shown in Figures 10 and 11. A linear arrangement has also been used and was in fact the configuration used to collect the data discussed in the next section, "Sample radiometer measurements".

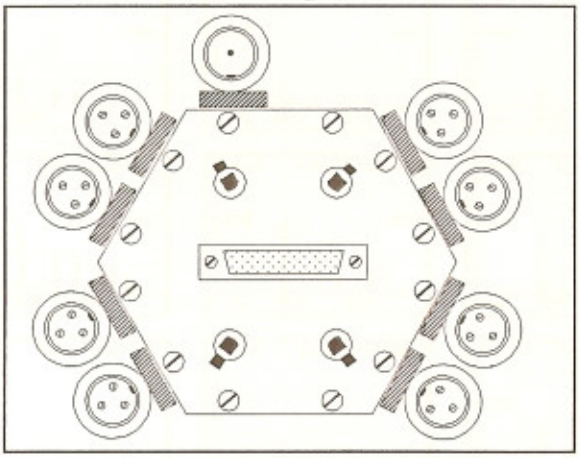

Figure 10: *Rear view of the 95C ultraviolet solar radiometer with DB25 connector. (For clarity the probe cables are not shown.)*

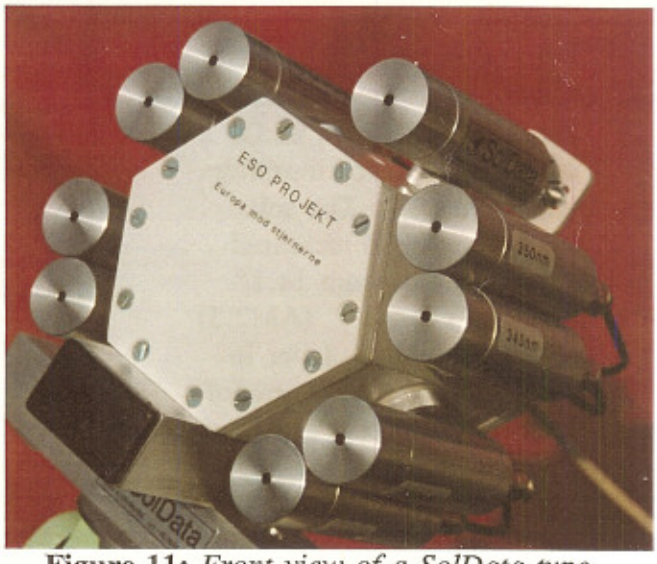

Figure 11: *Front view of a SolData type 95C ultraviolet solar radiometer.*

SAMPLE RADIOMETER MEASUREMENTS

A series of solar UV measurements were carried out in the 310 to 405 nm range during a period of clear weather in August, 1995. Figure 12 shows typical results for a 14 hour period on August 7th, a partly cloudy day in Silkeborg, Denmark (56.1°N). Probe calibration factors were obtained by means of Langley plots, i.e. extrapolations of terrestrial data for a range of air masses back to air mass zero (AM0). Excellent spectral irradiance data for extraterrestrial solar radiation is available from space flight measurements [9]. The ordinate units for the narrow-band graphs are $\mu W/(cm^2 \cdot nm)$.

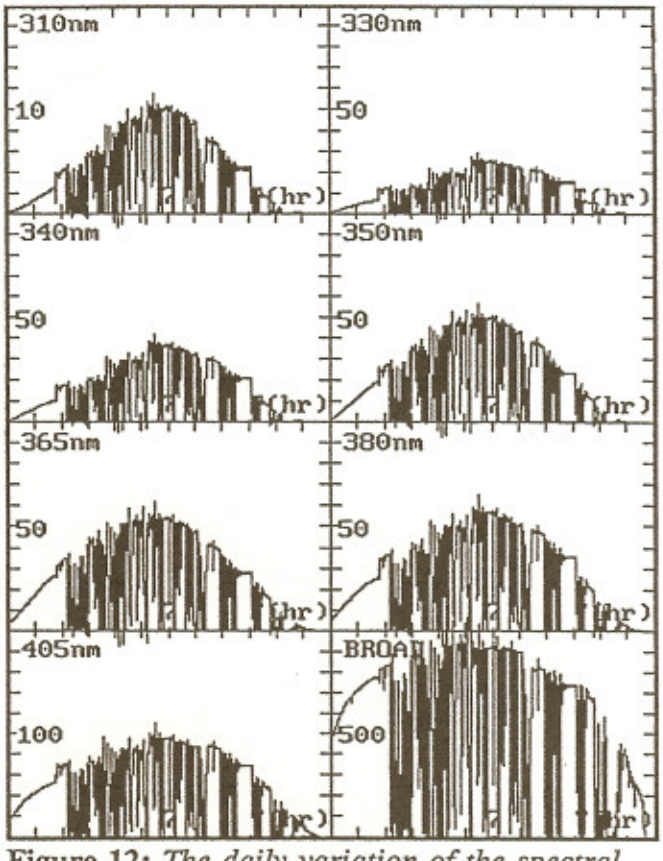

Figure 12: *The daily variation of the spectral irradiance in $\mu W/(cm^2 \cdot nm)$ at selected UV wavelengths is shown. Note that the graph marked BROAD has ordinate units W/m^2.*

Because the 310 nm radiation levels are low, an expanded scale has been used in this case. The graph marked BROAD refers to broad band detector measurements with the units W/m^2. During these preliminary runs slight adjustments of solar tracking were made every two hours. This caused slight discontinuities in the data.

Figure 13 shows bar charts of the solar UV spectrum at selected times during the measuring period.

The solar ultraviolet components change dramatically throughout the day. The upper three spectra were recorded at 07:30, 08:00 and 08:30 on the morning of August 7th. The solar elevation angle increased quite rapidly from 14.1° (AM3.7) to 22.4° (AM2.5) during the hour. Later in the day (the middle row of figures corresponds to 13:00, 14:00 and 15:00) the solar spectrum is more constant with the solar elevation angle reaching its maximum of 50.3°at 13:26. The air mass varied only

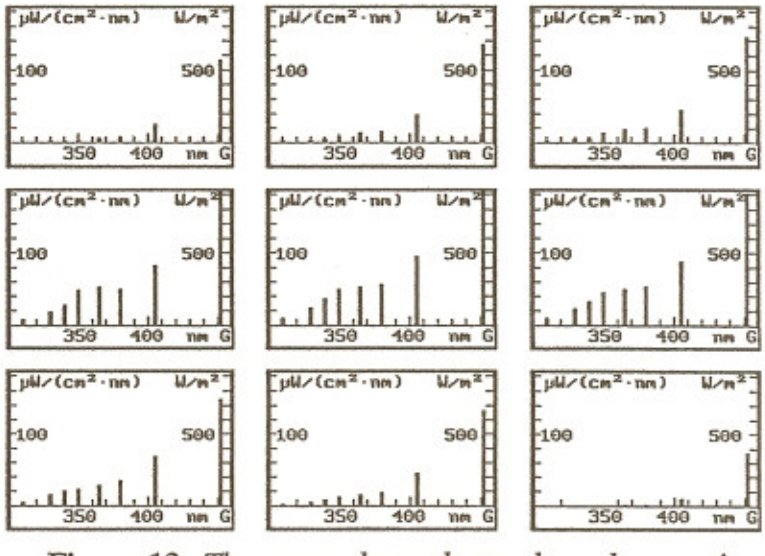

Figure 13: *The upper three charts show the morning solar UV spectrum (3.7>AM>2.5). The middle three are around solar noon (AM≈1.3), and the lower three show evening.*

slightly from AM1.3 to AM1.4 during this two hour period. Finally, the solar spectra at 17:30, 18:30 and 20:00 are shown with substantially attenuated ultraviolet components as the airmass value increases rapidly from AM2 to AM5.

The data processing strategy has been implemented using two computer programs: one designed for *data collection*, the other designed for *data analysis and display*.

Data collection

The program `RA1-STAR.EXT` records data from all eight probes about once per second. The data is averaged each minute and the standard deviation is computed. Data files consisting of 120 sets of minute-averaged data are saved at two hour intervals.

Data analysis and display

The second program `RA1-ANAL.EXT` loads the daily data files and performs data analysis and evaluation as required. Figures 12 and 13 were examples of the results of this analysis. A particularly valuable analysis consists of Langley plots of the collected data as shown in Figure 14.

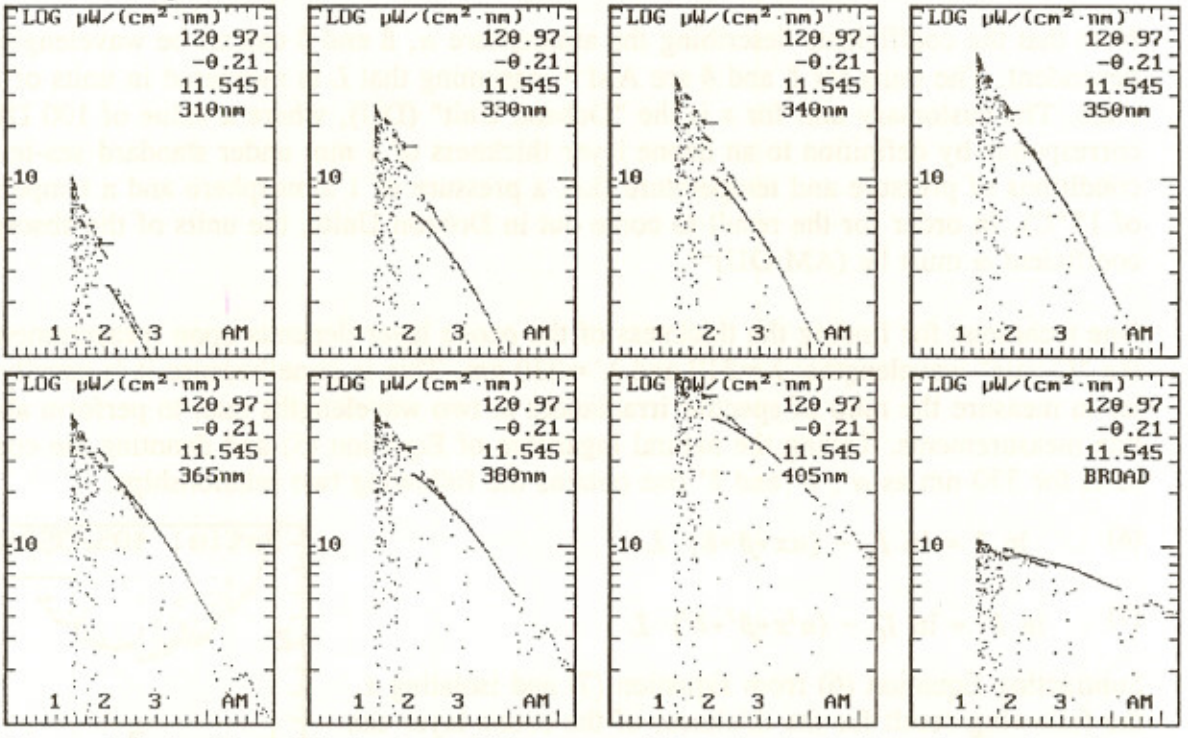

Figure 14: *Semilogarithmic plots of the spectral data for the indicated wavelengths are shown. It is the upper "edge" of the data corresponding to clear sky measurements which is of interest. If the probe calibration is correct, a line through these points extrapolated back to AM0 should indicate the UV spectral irradiance outside the earth's atmosphere.*

The values shown in Table I on the next page are available from the literature [9,10]. Furthermore, knowledge of these values permits the coefficient of absorption μ for the atmosphere to be computed for each of the measured wavelengths. Applying Lambert-Beers' law, where L is the path length of direct solar radiation in air mass units:

$$I_\lambda(L) = I_\lambda(0) \cdot e^{-\mu \cdot L}$$

The overall absorption coefficient μ can be broken down into terms corresponding to various atmospheric aerosols such as ozone, dust and particles and the remaining atmosphere. If one is interested, for example, in the thickness x of the ozone layer, an appropriate

λ	310	330	340	350	365	380	405	BROAD
$I_\lambda(0)$	68.9	105.9	107.4	109.3	113.2	112.0	164.4	1367
$I_\lambda(1.5)$	6.2	18.8	29.8	34.3	43.2	48.9	82.4	920
μ	1.61	1.15	0.85	0.77	0.64	0.55	0.46	0.26

Table I: *Published data is shown in $\mu W/(cm^2 \cdot nm)$ for the extraterrestrial AM0 solar spectral irradiance and for a clear AM1.5 atmosphere for each of the indicated wavelengths. The total atmospheric absorption coefficient μ is computed using Lambert-Beers' law. Note that the units for the broad-band radiation entries are W/m^2 and μ is in AM^{-1}.*

reformulation of Lambert-Beers' law would be [11]:

$$(5) \qquad I_\lambda(x) = I_{\lambda 0} \cdot e^{-\alpha x L - \beta L - \delta L}$$

Note that the coefficients describing the atmosphere α, ß and δ can all be wavelength dependent. The units for ß and δ are AM^{-1}, assuming that L is measured in units of air mass. The customary unit for x is the "Dobson Unit" (DU), where a value of 100 DU corresponds by definition to an ozone layer thickness of 1 mm under standard sea-level conditions of pressure and temperature (i.e. a pressure of 1 atmosphere and a temperature of 15°C). In order for the result to come out in Dobson Units, the units of the absorption coefficient α must be $(AM \cdot DU)^{-1}$.

One technique for finding the thickness of the ozone layer depends upon measurements of the "C-pair" wavelengths: λ=310 and λ'=330 nm. This is done because it is usually easier to measure the ratio of spectral irradiances at two wavelengths than to perform absolute measurements. Taking the natural logarithm of Equation (5) and denoting the coefficients for 330 nm as α', ß' and δ' one obtains the following two relationships:

$$(6) \qquad \ln I = \ln I_0 - (\alpha x + \beta + \delta) \cdot L$$

$$(7) \qquad \ln I' = \ln I_0' - (\alpha' x + \beta' + \delta') \cdot L$$

Subtracting Equation (6) from Equation (7) and isolating x, the following result for the thickness of the ozone layer can be found. Note that we have set $\delta - \delta' = 0$ because Mie scattering (from dust and other small particles) is only weakly wavelength dependent.

$$(8) \qquad x = \frac{\ln(I'/I) - \ln(I_0'/I_0)}{(\alpha - \alpha') \cdot L} - \frac{\beta - \beta'}{\alpha - \alpha'}$$

The air mass L can be computed based upon knowledge of the time of observation and the position of the observer on the earth's surface. The absorption coefficients α and ß are physical quantities which depend upon the atmosphere and in part upon the bandwidth of the measuring instrument.

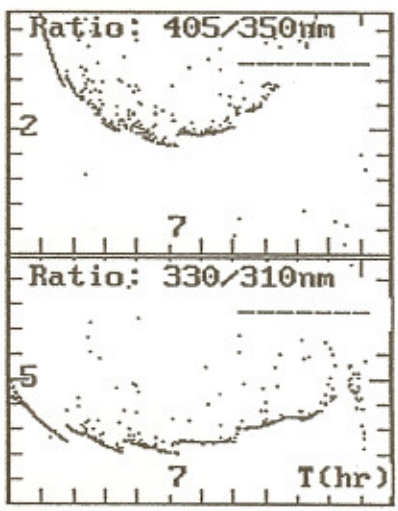

Figure 15: *Ratios I'/I are shown for a 14 hour period during August 7th.*

The ratio I'/I can be found from the UV solar radiometer data. Figure 15 shows ratios of 405 to 350 nm radiation as well at the radio for the C-pair: 330 to 310 nm radiation. The minima occur at solar culmination when short wave UV radiation levels are high.

CONCLUSION

In this paper we have directed our attention to the measurement of the spectral components of solar radiation in the 300-1100 nm region. The design and construction of a solar radiometer has been described. Specific measurements of a portion of the solar spectrum in and near the UVA spectral region have been carried out, and the results have been described. It has thus been demonstrated that it is possible to construct a simple solar radiometer with modest resources and to obtain useful results.

There are a number of important areas where such solar spectral measurements can be applied. The evaluation of the performance a photovoltaic cell, panel or system requires knowledge of the spectral irradiance of the source of illumination to which the photovoltaic devices will be exposed. Figure 16 shows how the response of a photovoltaic device varies with the air mass through which direct solar radiation passes. A solar radiometer can be useful in connection with the analysis of this interesting question. We have also illustrated how solar radiometry can be used to study the concentration atmospheric aerosols, for example ozone. Finally, the calculation of the ultraviolet exposure hazard under particular conditions of solar irradiance is an important application [12]. A more complete discussion of this important issue will be undertaken at a later date.

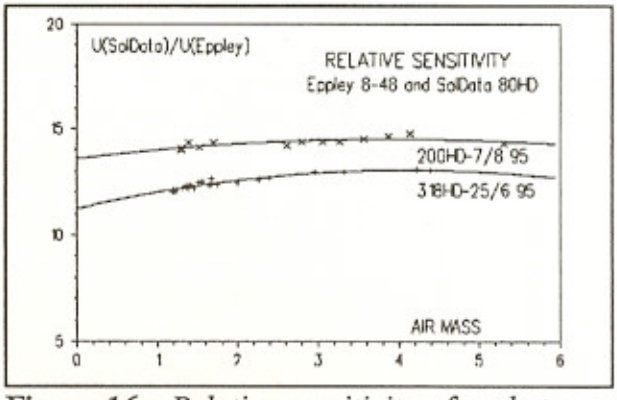

Figure 16:: *Relative sensitivity of a photovoltaic pyranometer vs. air mass.*

LITERATURE

[1] F.Bason, *Instruments for monitoring UV radiation (300-400 nm)*, K. MacGregor, C. Porteous, **Solar Energy at High Latitudes**, James&James Ltd., London, 1994.

[2] R.E. Bird, R.L. Hulstrom; *Terrestrial Solar Spectral Data Sets*, **Solar Energy 30**, no. 6, pp 563-573, 1982.

[3] G.H. Rieke, **Detection of Light from the Ultraviolet to the Submillimeter**, Cambridge University Press, Cambridge, 1994, Chapter 3.

[4] The photoconductive gain $G = \tau \cdot \mu \cdot E_x / \ell$, where τ is the carrier lifetime before recombination, μ is electron plus hole mobility, E_x is the strength of the internal field, and ℓ is the intercontact distance.

[5] The dual ND filter wheel is product number 5215 and is available from *New Focus Inc.*, 2630 Walsh Avenue, Santa Clara, CA 95051 USA (Fax:+1-408-980 8883).

[6] The IL1700 Research Radiometer is available from *International Light Inc.*, 17 Graf Road, Newburyport, MA 1950-4092 USA (Fax:+1-508-462 0759).

[7] G.H. Rieke, *op. cit.*, p. 56.

[8] Further information is available from the author (*SolData Technical Note 950815*).

[9] M.P. Thekaekara, *Solar Radiation Measurement: Techniques and Instrumentation*, **Solar Energy, 18**, pp 309-325, 1976.

[10] K.W. Böer, *The Solar Spectrum at Typical Clear Weather Days*, **Solar Energy, 19**, pp 525-538 (see DF/F data on p 535).

[11] Thormod Henriksen, Søren H.H. Larsen; **Ozonlaget og UV-stråling**, Institute of Physics, University of Oslo, Box 1048, N-0316 Oslo, Norway, pp 30-31.

[12] D.Sliney, M.Wolbarsht, Safety with Lasers and Other Optical Sources, Plenum Press, New York, 1980. See pp 170-177.

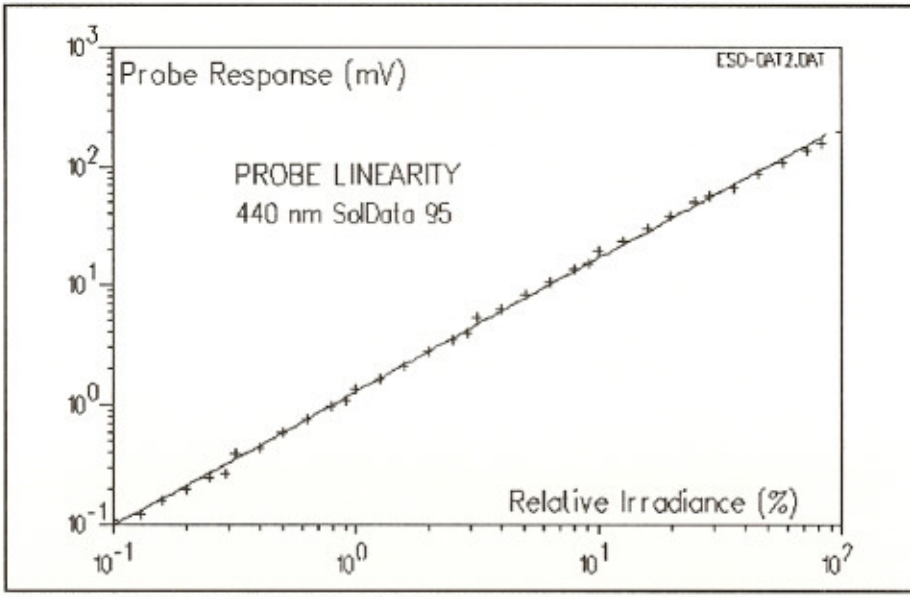

Figure 1 *Linearity check of 440 nm probe with a 150 W halogen light source and a pair of neutral density filter wheels.*

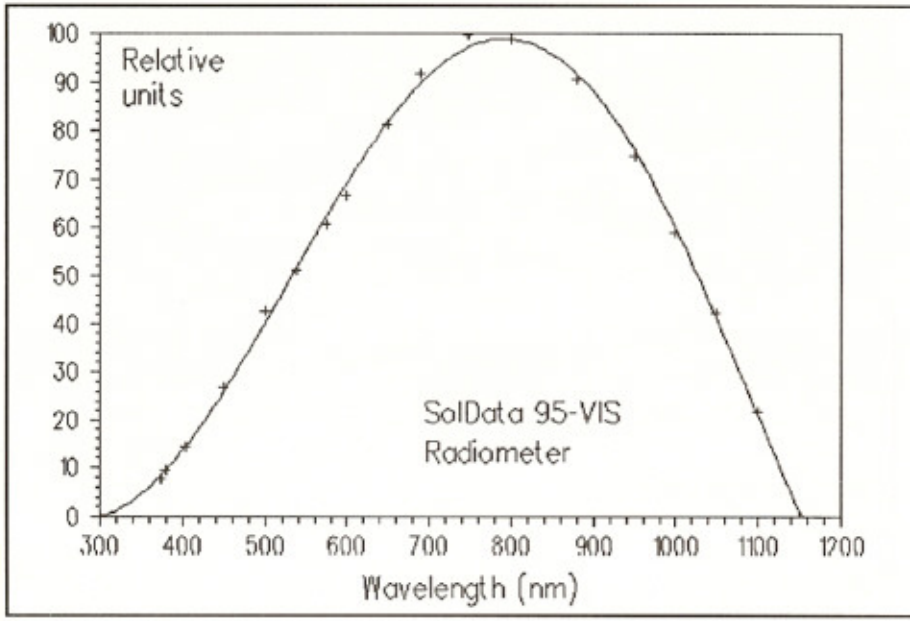

Figure 3 *The measured relative spectral response of the detector from 300-1200 nanometers is shown here.*